Numerical simulations of multiphoton ionization and above-threshold electron spectra

J. Javanainen
Department of Physics, University of Connecticut, Storrs, Connecticut 06268

J. H. Eberly and Qichang Su
Department of Physics and Astronomy, University of Rochester, Rochester, New York 14627
(Received 22 February 1988)

We study above-threshold ionization (ATI) of a one-dimensional model atom in a time-varying external laser field. The time-dependent Schrödinger equation is integrated in space and time using the Crank-Nicholson method, and the photoelectron energy spectrum is then computed by projecting the wave function onto the energy eigenstates of the time-independent zero-field Hamiltonian. We demonstrate an intensity-dependent ponderomotive shift of the ionization threshold, find a free-electron scaling of the number of ATI peaks with intensity and frequency of the field, and contrast the numerical simulations with two simple Keldysh-type models. For certain field parameters we encounter turn-on transients in the form of "energy-nonconserving" substructure within each ATI peak. Effects on the results of the physical parameters such as length and shape of the laser pulse on one hand, and of the iteration parameters on the other, are discussed in detail.

I. INTRODUCTION

In high-intensity photoionization of atoms a sequence of isolated peaks, separated by one photon energy, is observed in the energy spectrum of the liberated electrons, as if an electron continued to absorb photons even after it has been released from the atom.[1] This phenomenon is now commonly referred to as above-threshold ionization (ATI). The observation[2] that at high intensities the lowest peaks in the electron spectrum are suppressed relative to the more energetic ones (which is not consistent with finite-order perturbation theory) has prompted a large body of experimental[3-7] and theoretical[8-16] studies of ATI. For instance, recent experiments[4,5] on the angular distribution of photoelectrons and experiments with short pulses[6,7] reveal new aspects of ATI.

Even though it has been studied for ten years, ATI is not completely understood. Existing theoretical models differ in many respects, and typically ignore features of real experiments such as the temporal and spatial shape of the laser pulse, or most of the atomic structure, or both. At the same time, in different laboratories different electron spectrometers sometimes seem to give different results in nearly identical experiments, the temporal and spatial characteristics of the laser pulses are not always well in control, the space charge of the ions left behind may distort the electron spectrum, and so forth. It is difficult to judge how much weight should be put on agreement or disagreement between an experiment and a particular theory. Consequently, the experiments cannot easily distinguish between theories, and no consensus has been reached about the detailed mechanism of ATI.

The theme of the present work is to make numerical experiments related to laboratory experiments, but stripped as far as possible of inessential complications. We integrate the time-dependent Schrödinger equation[17,18] in space and time,[19] compute the photoelectron spectrum, and compare it with theoretical ideas. We emphasize that we do not aim at reproducing real experiments and their complexities, but rather at making unique experiments of our own. It is true that in this way we encounter physics which at the moment cannot be studied in real laboratories. We will be satisfied if our simple model provides some confirmation of qualitative tendencies and suggests possibilities for new experiments and theory.

In Sec. II we introduce our model, which consists of a one-dimensional atom in an external field. We describe the numerical procedure to solve the time-dependent Schrödinger equation for it and describe the methods used to calculate the electron spectrum. By contrasting a discrete numerical atom (constructed as a device to solve the Schrödinger equation) with the model atom with its continuous position coordinate, we can analyze the physical and mathematical aspects that govern the computation's accuracy. By comparing the results obtained with different square and smooth light pulses, we argue that results without a serious bias can be expected even for a short square pulse. This is a fortunate state of affairs, considering the cost of computations. Finally, we briefly mention the question of the $\mathbf{d}\cdot\mathbf{E}$ versus the $\mathbf{p}\cdot\mathbf{A}$ gauge of the dipole interaction.

In Sec. III we present results obtained by analyzing ATI spectra. We demonstrate in our simulations the threshold shift and channel closing that have been suggested[13,14] and partly verified[6,7] as the cause of the suppression of the lowest-energy peaks in the electron spectrum with increasing laser intensity. Second, we point out a free-electron scaling of the number of ATI peaks with the intensity and frequency of the field. We regard it as evidence in favor of the continuum-dressing mechanism[8-10,20] of ATI. Third, we compare the spectra from two Keldysh-type[8-10,20] final-state dressing models with our numerical experiments. Although the quantita-

tive agreement is bad, there is some qualitative resemblance between Keldysh-type predictions and our simulations.

In Sec. IV we present unusual photoelectron spectra that exhibit "energy-nonconserving" substructure within the usual ATI peaks. In our case (for contrast, see Ref. 7) the analysis shows that the extra peaks are transients associated with even a very smooth turn-on of the field. The remarks in Sec. V conclude the paper.

II. SIMULATION METHOD

A. Outline

Our numerical experiments are built around the Hamiltonian of a one-dimensional atom in an external field

$$H(t)=H_0-x\mathcal{E}(t)\sin(\omega t+\phi)\ , \tag{2.1}$$

where the "unperturbed" part is

$$H_0=-\frac{1}{2}\frac{\partial^2}{\partial x^2}+V(x)\ . \tag{2.2}$$

Here and below we use atomic units with $e=m=\hbar=1$.

At various stages of this work we have employed either one of two binding potentials of the atom: (i) the one-sided hydrogenic potential

$$V(x)=-1/x,\quad x>0\ , \tag{2.3a}$$

with reflecting boundary conditions at $x=0$ and (ii) the soft-core potential

$$V(x)=-\frac{1}{(1+x^2)^{1/2}}\ . \tag{2.3b}$$

The second of these has not been studied before, but it is in some respects a more realistic model for multiphoton ionization studies. Both potentials have a Coulomb tail, and consequently the high-lying bound eigenstates of H_0 have a Rydberg series structure. Both models represent atomlike quantum systems governed by a complete Hamiltonian, and hence satisfy sum rules similar to real three-dimensional atoms. The soft-core model (2.3b) possesses the additional advantages that parity is a good quantum number, and its bound states do not have permanent dipole moments. In this respect it is more realistic than one-sided hydrogenic models. One may view parity as the one-dimensional remnant of three-dimensional angular momentum and contend that in model (2.3b) the dipole moment selection rules are analogous to those of three-dimensional atoms. In this paper our discussion will be restricted to this model unless otherwise noted.

The envelope of the electric field will either be characteristic of a square pulse:

$$\mathcal{E}(t)=\begin{cases}\mathcal{E}_0, & 0\le t\le T\ ,\\ 0 & \text{otherwise}\ ,\end{cases} \tag{2.4a}$$

or a smooth pulse

$$\mathcal{E}(t)=\begin{cases}\mathcal{E}_0\sin^2\left[\dfrac{\pi t}{T}\right], & 0\le t\le T\\ 0 & \text{otherwise}\ .\end{cases} \tag{2.4b}$$

The phase of the electric field ϕ is chosen zero, unless otherwise noted.

In essence we first find the eigenvalues W and eigenvectors $|W\rangle$ of the unperturbed Hamiltonian H_0. Next, we integrate the time-dependent Schrödinger equation with the full Hamiltonian $H(t)$ in space and time over the desired pulse duration T, starting from the ground state of H_0. Subsequently we project the wave function onto the (typically but not necessarily positive-energy) eigenstates $|W\rangle$ to obtain the photoelectron energy spectrum

$$P(W;T)=|\langle W|\psi(T)\rangle|^2\ . \tag{2.5}$$

The last step is to investigate and interpret the spectra in terms of pulse duration, intensity, wavelength, etc.

The technical implementation of this procedure is described in Sec. II B. In Sec. II C we discuss the relation of our necessarily discrete computations to the desired solution of the continuous-variable space-time Schrödinger equation and in particular enumerate factors that determine the truncation errors. Two partly practical and partly physical issues that we wish to regard here as part of the solution methodology, the effects of the pulse length and pulse shape and of the gauge of the electromagnetic field, are investigated in Secs. II D and II E, respectively. Finally, in Sec. II F we list certain limitations on the parameters in our calculations, the reason for which is currently not understood.

B. Practical computations

1. *Conversion to the* $\mathbf{p}\cdot\mathbf{A}$ *gauge*

The wave function of the ionized electron is obviously going to spread out as a function of time. In this sense the dipole interaction, which is proportional to x, will grow without bound, and numerical problems might ensue. Therefore we first convert the Hamiltonian to the $\mathbf{p}\cdot\mathbf{A}$ gauge of the dipole interaction. As the A^2 term can be absorbed in a phase factor that has no bearing on occupation probabilities, the new Schrödinger equation for the correctly transformed effective wave function reads

$$i\frac{\partial}{\partial t}\psi'(x,t)=\left[H_0+iA(t)\frac{\partial}{\partial x}\right]\psi'(x,t)\ . \tag{2.6}$$

The momenta have an upper limit in practice (as do the electron energies), so loosely speaking the $\mathbf{p}\cdot\mathbf{A}$ interaction is bounded. Here

$$A(t)=-\int_0^t\mathcal{E}(t)\sin(\omega t+\phi)dt \tag{2.7}$$

is the vector potential in the gauge with $A(t)=0$ at $t=0$. The relation between the $\mathbf{d}\cdot\mathbf{E}$ and $\mathbf{p}\cdot\mathbf{A}$ wave functions ψ and ψ' is well known:

$$\psi(x,t)=e^{-ixA(t)}\psi'(x,t)\ . \tag{2.8}$$

To obtain the final results in the $\mathbf{d}\cdot\mathbf{E}$ gauge one should

first convert the initial ground-state wave function of H_0 to the $\mathbf{p}\cdot\mathbf{A}$ gauge [for the particular form of the vector potential (2.7) nothing needs be done], do the time integration of (2.6), and then convert the outcome back to $\mathbf{d}\cdot\mathbf{E}$ before taking the inner product (2.5).

2. Discretization of the Schrödinger equation

The next step is to discretize the wave functions and the operators acting on them. Instead of the continuous wave function $\psi(x)$ we utilize an $N+1$ dimensional vector $\psi_n=\psi(x_n)$ whose components represent the wave function at the points $x_n=n\delta x$, for $n=-N/2$ to $N/2$. The discrete counterpart of the time-independent Hamiltonian is defined by the expression

$$(H_0\psi)_n=-\frac{1}{2(\delta x)^2}(\psi_{n+1}-2\psi_n+\psi_{n-1})+V(x_n)\psi_n\ , \tag{2.9}$$

and the $\mathbf{p}\cdot\mathbf{A}$ interaction is represented by

$$(-\mathbf{p}\cdot\mathbf{A}\psi)_n=\frac{iA}{2\delta x}(\psi_{n+1}-\psi_{n-1})\ . \tag{2.10}$$

Both of these approximations of the derivatives are accurate to second order in δx. We use reflecting boundary conditions at both ends of the integration region. Hence the declarations

$$\psi_{-N/2-1}=\psi_{N/2+1}=0 \tag{2.11}$$

are always understood in our formulas.

3. Energy eigenvalues and eigenfunctions

In the discrete representation the matrix of the time-independent Hamiltonian is tridiagonal. We use the standard QL algorithm[21] to find the eigenvalues. Widely available routines can also compute the eigenvectors. However, we do not need all eigenvectors, and how many are needed is decided later.

To generate an individual eigenvector ψ_n^k corresponding to any approximate eigenvalue $\tilde{W}_k$ we therefore employ the "inverse iteration" method.[21] We repeatedly solve the linear equations

$$(H_0-\tilde{W}_k)\psi^k(i+1)=\psi^k(i) \tag{2.12}$$

beginning with a random initial vector $\psi^k(0)$. How it works can be seen by writing the solution to (2.12) in the eigenstate basis as

$$|\psi^k(i+1)\rangle=\sum_n\frac{|W_n\rangle\langle W_n|}{W_n-\tilde{W}_k}|\psi^k(i)\rangle\ . \tag{2.13}$$

If $\tilde{W}_k$ is a good approximation to a true eigenvalue W_k, the projections in (2.13) amplify the $|W_k\rangle$ component of vector $|\psi^k(i)\rangle$ at the expense of the others.

Because parity is a good quantum number, the eigenstates can be chosen either even or odd; in fact, the energy eigenstates $n=0,1,\ldots$ are alternately even and odd. The ground state is even. In Table I we list the energies of the lowest 10 discrete states obtained for $\delta x=0.707$ and $N=32$ K. The results should coincide with the corresponding energies of the continuous atom to within about ±1 in the last digit displayed. We show in Fig. 1 a plot of the lowest eigenenergies against $1/(n+1)^2$, verifying their rapid approach to Rydberg scaling.

TABLE I. Notation, energy, and symmetry under inversion of the ten lowest-energy bound states of our one-dimensional model atom with the binding potential $V(x)=-(1+x^2)^{-1/2}$, $x=(-\infty,\infty)$. The energies are accurate to about ±1 in the last digit displayed.

Level index n	Energy W	Even/odd
0	−0.669 8	+
1	−0.274 9	−
2	−0.151 5	+
3	−0.092 70	−
4	−0.063 54	+
5	−0.045 50	−
6	−0.034 61	+
7	−0.026 89	−
8	−0.021 71	+
9	−0.017 73	−

4. Time evolution

A time step δt of the wave function is carried out according to[19]

$$\psi(t+\delta t)=\left[1-\frac{i\delta t}{2}H\left[t+\frac{\delta t}{2}\right]\right]\times\left[1+\frac{i\delta t}{2}H\left[t+\frac{\delta t}{2}\right]\right]^{-1}\psi(t)\ . \tag{2.14}$$

This is a second-order approximation, i.e., the error is of

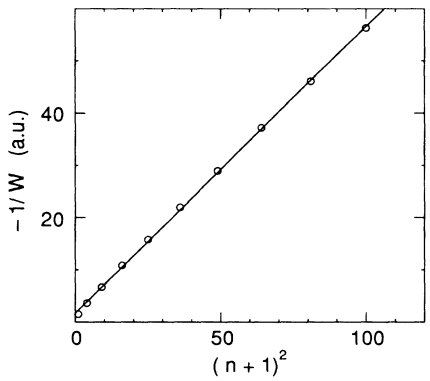

FIG. 1. $-1/W$ for the ten lowest bound-state energies W (○) of our one-dimensional soft-core atom plotted against the function $(n+1)^2$ of the index $n=0,1,\ldots$ labeling the states. The solid line is the linear least-squares fit. Rydberg scaling of the energy levels is evident.

the order $(\delta t)^3$. In fact, (2.14) is a trivial generalization of the familiar Crank-Nicholson algorithm[21] to the case when the parameters of the partial differential equation depend on time.

5. *Implementation of the computations*

It is evident from (2.12) and (2.14) that solving a set of linear equations with a tridiagonal matrix is the bottleneck of the computations. We started the computer work on a CDC Cyber 180/990, a fast scalar machine. The solution was implemented with a well-known simple form of Gaussian elimination for tridiagonal equations. This algorithm does not vectorize, however, so we abandoned it when the computations were transferred to a Cyber 205 supercomputer with two vector pipes.

Currently we resort to cyclic reduction.[21] The idea is to combine the original equations in such a way as to eliminate every second one of them, so that the remaining ψ_n couple to ψ_{n-2} and ψ_{n+2}. This process is repeated until the number of equations is so small that the scalar Gaussian elimination is faster than continuing to cut down the number of equations. We usually let the number of equations run down to one or two. After the remaining equations have been solved, the process is reversed; the known values of ψ_n and ψ_{n+2m} are used to generate the intermediate ψ_{n+m}. The method applies to any set of tridiagonal equations, and it vectorizes. Unfortunately, it also involves repeated compression and decompression of data, and tricky bookkeeping. Even though we implemented the algorithm in the explicit vector code of the Cyber 205, the cyclic reduction solution turned out to be only six or seven times faster than the Gaussian elimination in real-valued problems, and two or three times faster with complex vectors.

There are a number of other differences between the implementations of the computations on these two machines. In this paper we always describe our current methods, even though many of the results still date back to the Cyber 180/990 and may have been obtained differently. We have checked that the alterations in the algorithms should not produce changes in the results comparable to the uncertainties resulting from the truncation errors.

In the computations reported below the iteration parameters vary greatly. Before entering a more detailed discussion, we want to give an impression of the parameters that constitute the present practical limits: $N=32$ K, $\delta x=0.07$, $\delta t=0.08$, and number of time steps $N_T=16$ K. The integration region thus extends the distance $D=\delta x N/2\sim 1000$ a.u. to either side of the origin, and the pulse time is $T=\delta t N_T\sim 1000$ a.u. About four inverse iteration steps are needed to extract an eigenvector such that the probabilities of the undesired contamination states are below 10^{-8}.

C. Discrete computations versus the continuum problem

With the reflecting boundary conditions (2.11) the discretized unperturbed Hamiltonian (2.9) and the perturbation (2.10) are Hermitian operators in the Hilbert space of $N+1$ dimensional complex vectors. The discretized atom introduced as a solution method for the continuous Schrödinger equation is a quantum system in its own right. But, as we utilize the discrete atom to approximate the continuous atom rather than as an independent object of study, the connection between the two has to be laid down.

1. *Spectrum of the Hamiltonian*

The discrete atom has a finite number $N+1$ of eigenstates. The number of the Rydberg levels is finite, and there are no true continuum states.

The spatial size of a hydrogenic Rydberg level with principal quantum number n is of the order n^2. On the other hand, the natural n for the Rydberg series of our discrete atom to terminate is such that the wave function extends to the reflecting boundary. This leads to the estimate $n\sim D^{1/2}\sim 30$ for the number of negative-energy eigenstates of the discretized atom, which is borne out in our numerical studies. The ground state falls at $W=-0.670$.

To investigate the positive-energy spectrum of the discretized atom we temporarily ignore the binding potential. The energy eigenvalues are then found to be

$$W_k=\frac{1}{(\delta x)^2}\left[1-\cos\frac{k\pi}{N+2}\right],\quad k=1,\ldots,N+1\ . \tag{2.15}$$

In the limit of large N the energy may be regarded as a continuous function of k, and the level density is approximated as

$$\frac{\partial k}{\partial W}=\frac{N\delta x}{\pi\sqrt{2W}\,[1-(\delta x)^2W/2]^{1/2}}\ . \tag{2.16}$$

Were it not for the second square root in the denominator, (2.16) would be the familiar asymptotic approximation $(N\to\infty)$ of the energy level density in a box of length $N\delta x$ for a free particle with a continuous position variable. The discreteness of the grid of x does not essentially perturb the energy spectrum for energies W satisfying

$$\delta x\sqrt{W}\ll 1\ . \tag{2.17}$$

Note that $\sqrt{2W}$ is the momentum of an electron with energy W, so (2.17) requires that the de Broglie wavelength of the electron be much longer than the grid spacing. This is precisely what one might have expected in the first place.

When the binding potential $V(x)$ is included, a small number (say 30 out of 30 K) of levels are split off from the positive-energy band and are pulled down to negative energies. Except in the immediate vicinity of the threshold where the continuum approximation leads to a spurious divergence, (2.16) turns out to be a good approximation to the density of positive-energy levels. The number of energy eigenstates up to $W=1$ is of the order 1000.

2. *Time dependence*

Imagine next that the Schrödinger equation were integrated exactly both for the discrete atom and for the true continuous atom. The question is, under what con-

ditions can the discreteness be ignored in the time evolution of the wave functions.

Qualitatively, the difference between a discrete and a continuous spectrum should not show for short interaction times when the discrete levels cannot be resolved, i.e., when the observation time T and level density $\partial k/\partial W$ satisfy

$$T\frac{\partial W}{\partial k} \lesssim 1 \ . \tag{2.18}$$

Using (2.16), we have

$$T\sqrt{2W} \lesssim N\delta x \ . \tag{2.19}$$

Another obvious condition is that the wave packet that started propagating from the origin at $t=0$ must not yet have hit the reflecting boundary at time T. But, with the recognition that the velocity of an electron with energy W is $\sqrt{2W}$, this condition too boils down essentially to (2.19).

3. *Definition of the photoelectron energy spectrum*

In the continuous case, when the continuum eigenstates are energy normalized,

$$P(W)dW = |\langle W \mid \psi \rangle|^2 dW$$

gives the probability of finding the electron in the energy interval $[W, W+dW)$.

In the discrete case we define the photoelectron spectrum as

$$P(\tfrac{1}{4}(W_{i-1}+W_i+W_{i+1}+W_{i+2})) = \frac{|\langle W_i \mid \psi \rangle|^2}{W_{i+1}-W_{i-1}} + \frac{|\langle W_{i+1} \mid \psi \rangle|^2}{W_{i+2}-W_i} \tag{2.20}$$

at the energies appearing on the left-hand side, and by linear interpolation for the energies between these points. On the right of (2.20) we have averaged over the populations of the alternating even and odd eigenstates of the discrete atom, which may have vastly different populations. The integral of $P(W)$ from (2.20) over an energy region containing discrete eigenvalues approximates the sum of the populations of those eigenstates, the better the more slowly varying $P(W)$ is as a function of W, and the larger the number of eigenvalues is. Equation (2.20) is a justifiable analog of the continuum-electron spectrum for the discrete atom.

For a neutral atom the oscillator strength per unit energy interpolates continuously across the ionization threshold,[22] and no finite measurement time allows for an exact determination of the accumulation point of the Rydberg series. In this sense nothing abrupt happens at the ionization threshold. Equation (2.20) is defined as a *mathematical* formula beginning from the average of the energy of the lowest four eigenstates. Our message is that it has *physical* content at negative energies, too: It is natural to define a continuous energy spectrum using (2.20) all the way down the Rydberg states which cannot be resolved from their neighbors during the given interaction time and which therefore still behave like a continuum.

4. *Convergence of time integration*

The remaining technical question of the numerical integrations is the convergence of the time-stepping algorithm with varying δt. The operator on the right-hand side of (2.14) is unitary, both in quantum mechanics with a continuous position variable and for our discretized atom. All eigenvalues of the time-stepping operator have unit modulus, and repeated time stepping cannot amplify anything (errors included) exponentially. In other words, the algorithm of (2.14) is numerically stable.

To estimate the truncation error derived from the finite value of δt we study the evolution of the eigenvector $|W_k\rangle$ of the discretized unperturbed Hamiltonian H_0. Exact time evolution over $T=N_T\delta t$ simply multiplies the state by the phase factor $\exp(-iTW_k)$, whereas N_T repeated applications of the time-stepping algorithm give

$$|\psi(T)\rangle = \left[\frac{1-(i/2)\delta t W_k}{1+(i/2)\delta t W_k}\right]^{N_T} |W_k\rangle \ . \tag{2.21}$$

Both ways, just a phase factor is attached to the wave function. Now, the ratio of these phase factors may be written

$$e^{i\xi} = \left[\frac{\exp\left[\frac{i\delta t}{2}W_k\right]\left[1-\frac{i\delta t}{2}W_k\right]}{\exp\left[-\frac{i\delta t}{2}W_k\right]\left[1+\frac{i\delta t}{2}W_k\right]}\right]^{N_T} , \tag{2.22}$$

which after expanding the fraction in δt and using the limit

$$\lim_{N\to\infty}\left[1+\frac{x}{N}\right]^N = e^x \tag{2.23}$$

gives an approximate expression for the phase ξ,

$$\xi \sim \tfrac{1}{12} T W_k (\delta t W_k)^2 \ . \tag{2.24}$$

The phase error over the whole significant range of energies W should be uniformly smaller than or of the order of one, which gives a condition on δt

$$\delta t \lesssim \frac{1}{W}\left[\frac{12}{TW}\right]^{1/2} . \tag{2.25}$$

5. *Final choice of computation parameters*

The only way to find out for sure if the integration parameters result in a tolerable error in the photoelectron spectrum is to vary them and analyze how the result changes. This is, unfortunately, a very laborious and expensive procedure which cannot be done routinely. Instead, we generally test the accuracy at extreme values of the parameters (say, the highest intensity in a series of spectra at different intensities) and when we want to rule out truncation errors as a possible source of a qualitative feature in the results.

Nonetheless, we do have a few analytic conditions. Equation (2.17) states that the *grid should be dense*

enough to hold the de Broglie wave for the highest relevant electron energy and gives a condition on the spatial step δx. Equation (2.19) demands that the *wave packet propagating from the origin must not hit the reflecting boundary during the given interaction time* T and thus determines the number of spatial points N. Finally, (2.23) which ensures that the *discrete time evolution formula does not cause a large phase error in the relevant energy states,* dictates the time step δt.

We have indications from early phases of this work that accurate *wave functions* are obtained only at smaller $[\delta t \sim (\delta x)^2]$ time steps than is our current practice. However, we have found by starting from such time steps and then repeatedly doubling δt that, somewhat mysteriously, the *electron spectra* are much less sensitive to the time step than the wave functions.

In principle, round-off errors of the computer should also be considered. However, we have carried out all computations in 64-bit double precision and have not encountered round-off errors that would rival the truncation errors.

D. Effects of pulse length and shape

1. Square-pulse data

We begin by examining the photoelectron spectra at different interaction times, first for different length square pulses. We obtain ATI peaks, and they exhibit features not observed in experiments: They move, split, and recombine in the short time scale of one field cycle. Figure 2 shows the electron spectra for times T corresponding to 8, $8\frac{1}{8}$, $8\frac{1}{4}$, $8\frac{3}{8}$, and $8\frac{1}{2}$ cycles of the external field for $\omega=0.148$ (five-photon ionization) and $\mathcal{E}_0=0.05$ ($\sim 10^{14}$ W cm^{-2}).

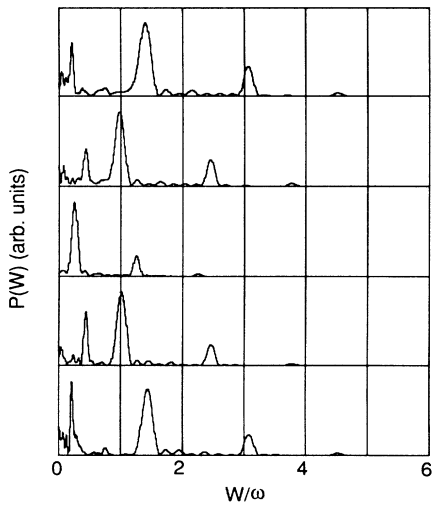

FIG. 2. Electron spectra for the field frequency $\omega=0.148$ (five-photon ionization) for a square pulse with field strength $\mathcal{E}_0=0.05$ ($\sim 10^{14}$ W cm^{-2}), at times $T=339.63$, 344.94, 350.25, 355.55, and 360.86 corresponding to 8, $8\frac{1}{8}$, $8\frac{1}{4}$, $8\frac{3}{8}$, and $8\frac{1}{2}$ cycles of the external field (from top to bottom). The integration parameters are $N=32\,766$, $\delta x=0.707$, and $\delta t=0.082\,917\,9$. The total ionization probability under the curve of the middle graph for the $8\frac{1}{4}$ cycle interaction time is 3.3×10^{-2}.

This feature also appears in one-sided atom models where the peaks do not split and the explanation is easier to uncover. Following multiphoton absorption, in addition to flying away from the atomic core at a roughly constant speed, the electron undergoes forced oscillations in the external field $\mathcal{E}_0\sin\omega t$ at the velocity $v(t)=-(\mathcal{E}_0/\omega)\cos\omega t$. It is this quiver motion that deforms the spectra in Fig. 2. The quiver velocity may be anticipated to be zero at times corresponding to $n+\frac{1}{4}$ and $n+\frac{3}{4}$ cycles of the field when $\cos\omega t=0$. Indeed, these are the times at which the computed spectra have peak spacing equal to one photon energy. The magnitude of the peak motion also agrees with that predicted for the quiver motion. The splitting in Fig. 2 ensues because for a two-sided atom model (both positive and negative spatial coordinates x included) each peak in the unsplit spectrum at $8\frac{1}{4}$ cycles corresponds to a roughly half-and-half mixture of electrons flying away from the origin in the + and − directions. At any given time the quiver motion, whose velocity amplitude is the same for all electrons, adds energy to half of the electrons and subtracts it from the other half.

The picture of the quiver motion is further confirmed in Fig. 3 which gives the spectra for varying phases of the field $\mathcal{E}_0\sin(\omega t+\phi)$ with (a) $\phi=0$ and (b) $\phi=\pi/4$. The spectra are taken at times corresponding to $8\frac{3}{4}$ and 9 cycles of the external field, respectively, when the quiver velocity $-(\mathcal{E}_0/\omega)\cos(\omega t+\phi)$ should be zero. They are nearly identical. The phase at which the field is turned on does not play a significant role for these field parameters, as long as the spectrum is also recorded at a properly shifted phase.

In Fig. 4 we plot the spectra for $4\frac{1}{4}$, $8\frac{1}{4}$, $16\frac{1}{4}$, and $32\frac{1}{4}$ cycles of the field, again for $\omega=0.148$ and $\mathcal{E}_0=0.05$, and some of the corresponding numerical data are given in

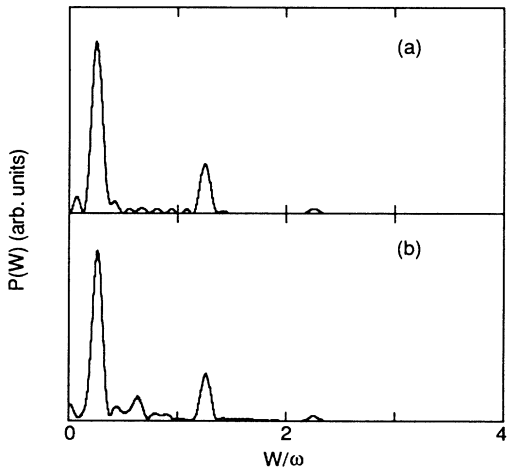

FIG. 3. Spectra for the field $\mathcal{E}_0\sin(\omega t+\phi)$ with (a) $\phi=0$ and (b) $\pi/4$, each for $\omega=0.148$ and $\mathcal{E}_0=0.05$. The spectra are given at times corresponding to $8\frac{3}{4}$ and 9 cycles of the field, respectively.

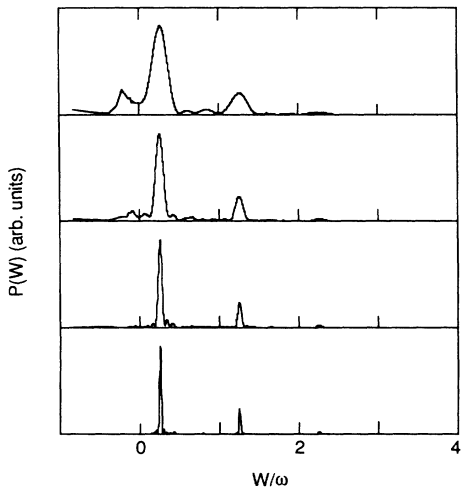

FIG. 4. Spectra for square pulses with $\omega=0.148$ and $\mathcal{E}_0=0.05$, for $4\frac{1}{4}$, $8\frac{1}{4}$, $16\frac{1}{4}$, and $32\frac{1}{4}$ cycles of the field (from top to bottom). A detailed breakdown of the peak positions, etc., is given in Table II.

Table II. The peaks narrow with increasing interaction time, but their positions and relative heights are practically the same at all these times. Assuming exponential decay of the ground state to the continuum, the respective ionization probabilities (areas under the curves for $W\geq 0$) would correspond to the ionization rates 4.5, 4.1, 3.9, and 3.8×10^{-3}/cycle. A small drift is discerned as if there were an initial burst of nonexponential excess ionization, but we do not know how much of the effect is real and how much numerical errors. Since the total ionization is small even after $32\frac{1}{4}$ cycles, the widths of the peaks might simply derive from the finite interaction time. In fact, the full widths at half maximum $\Delta\nu$ give for the lowest-energy peaks in Fig. 4 the products $T\Delta\nu=5.9$, 5.8, 5,7, and $5.9\sim 2\pi$.

Our experience is that if there is going to be an ATI spectrum at all, it usually materializes in about two or three field cycles. Thereafter the positions and relative heights of the ATI peaks remain largely unchanged if taken at times when the quiver motion comes to a halt. In spite of our deliberate attempts to produce an exception to this rule, we have only come across the one that is presented in Fig. 5. Again we choose $\omega=0.148$ but the intensity is higher than before, $\mathcal{E}_0=0.1$ ($\sim 4\times 10^{14}$ W cm^{-2}). We plot the spectra for $4\frac{1}{4}$, $8\frac{1}{4}$, and $32\frac{1}{4}$ cycles of the field, and include a portion of negative-energy Rydberg states. Between $4\frac{1}{4}$ and $8\frac{1}{4}$ cycles of the field the "photoelectron" peak in the Rydberg states gets lifted up into the continuum and is seemingly dumped predominantly to the lowest above-threshold peak.

The oscillations in the spectrum conform to the velocity $v(t)=-(\mathcal{E}_0/\omega)\cos\omega t$ which is the solution for *adiabatic*, not sudden, turn-on of the driving force $\mathcal{E}_0\sin\omega t$. The invariance of the peak positions and relative heights with respect to the turn-on phase of the field and the interaction time confirm the picture that the electron leaks out of the atom continuously, and in so doing emerges locked to the adiabatic quiver velocity. The spectra should be taken at times when the quiver motion has come to a standstill, because then only the drift motion remains and carries clean information about the ionization.

2. *Smooth-pulse response*

To take the electron spectra at times corresponding to $n\pm\frac{1}{4}$ cycles of the external field may sound somewhat artificial. To dispel the associated doubts we have carried out comparisons between spectra obtained with various length square and smooth pulses. An example, the ATI spectrum with a $32\frac{1}{4}$-cycle square pulse and after a 32-cycle smooth pulse, is presented in Fig. 6 for $\omega=0.148$ and $\mathcal{E}_0=0.1$. To the extent that the peak positions for

TABLE II. Numerical data of the electron spectra for $\omega=0.148$ and $\mathcal{E}_0=0.05$ at times T corresponding to $4\frac{1}{4}$, $8\frac{1}{4}$, $16\frac{1}{4}$, and $32\frac{1}{4}$ cycles of the external field, as plotted in Fig. 4. The iteration parameters are $N=32\,766$, $\delta x=0.0707$, and $\delta t=0.082\,917\,9$.

Cycles in square pulse	$4\frac{1}{4}$	$8\frac{1}{4}$	$16\frac{1}{4}$	$32\frac{1}{4}$
Interaction time T	180.43	350.25	689.88	1369.14
Total ionization	0.019	0.033	0.061	0.114
Average energy[a] $\langle W\rangle$	0.076	0.077	0.078	0.077
Position[b] of lowest peak W_0	0.040	0.037	0.037	0.037
Position[b] of second peak W_1	0.187	0.185	0.185	0.185
Position[b] of third peak W_2	0.333	0.333	0.333	0.333
W_0/ω	0.268	0.252	0.252	0.252
W_1/ω	1.266	1.249	1.249	1.249
W_2/ω	2.251	2.251	2.251	2.251
Height of lowest peak	0.387	1.235	4.681	17.698
Height of second peak	0.095	0.339	1.308	5.043
Height of third peak	0.009	0.034	0.128	0.459
Lowest peak FWHM $\Delta\nu$	0.0326	0.0167	0.0082	0.0043

[a]$\langle W\rangle$ is defined in Eq. (3.2).

[b]Position stands for the argument W giving the maximum of the peak of $P(W)$.

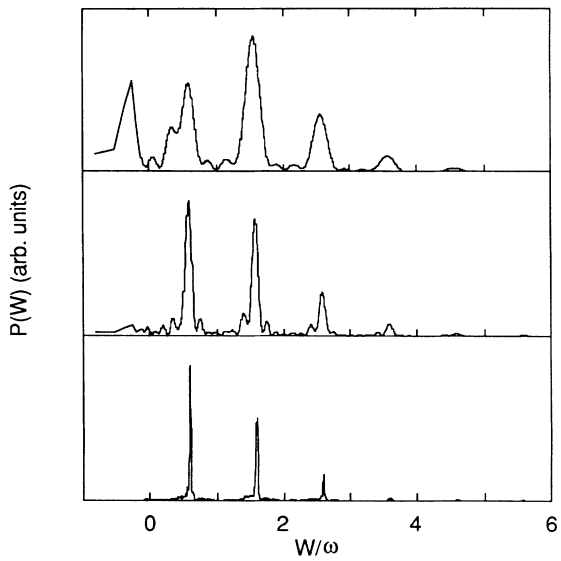

FIG. 5. Spectra for square pulses with $\omega=0.148$ and $\mathcal{E}_0=0.1$ ($\sim 4\times 10^{14}$ W cm^{-2}), at $4\frac{1}{4}$, $8\frac{1}{4}$, and $32\frac{1}{4}$ cycles of the field. The ionization probability for the $8\frac{1}{4}$-cycle interaction time is 0.63.

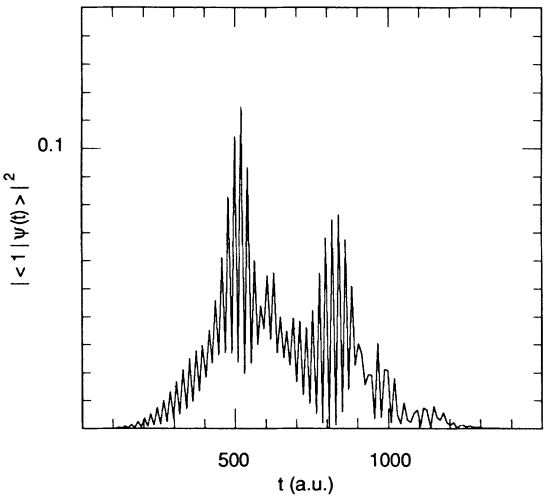

FIG. 7. Population of the first excited state of the atom as a function of time for a 32-cycle smooth pulse with $\omega=0.148$ and $\mathcal{E}_0=0.1$. A resonance is apparent at times $t=520$ and 840.

the smooth pulse can be defined meaningfully, they are qualitatively the same as for the square pulse. Also, the relative heights of the ATI peaks appear to be roughly the same.

One possibly undesirable feature of smooth pulses also is evident in Fig. 6(b). The peaks are broader than for a square pulse and may have a fuzzy substructure. Another source of potential complications with smooth pulses can be detected by plotting the population of the first excited state ($n=1$) as a function of time, as in Fig. 7. At times $t=520$ and 840, with the field strength $\mathcal{E}(t)=0.087$, the dynamic Stark shifts have rendered a resonance between the ground state and the first excited state. It apparently is a three-photon resonance with frequency 0.4440, close enough to the zero-field frequency 0.3949 between these states.

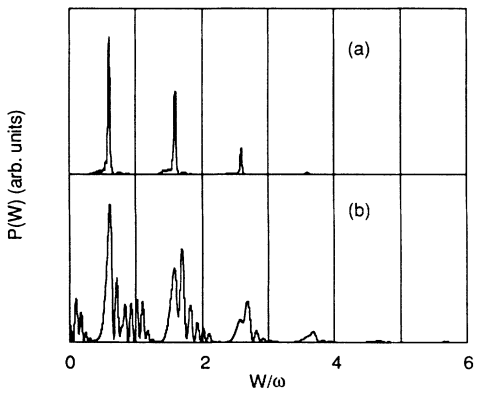

FIG. 6. ATI spectra for a $32\frac{1}{4}$-cycle square pulse (a), and after a 32-cycle smooth pulse (b), for $\omega=0.148$ and $\mathcal{E}_0=0.1$. The respective areas under the curves are 0.94 and 0.57.

3. *Summary of pulse shape and length considerations*

At present we use the smooth pulse only when there are good reasons to believe that the smoothness may essentially influence the physics. For routine ATI spectra this is not the case. One can simply take the square-pulse spectrum at a time when the quiver motion has come to a standstill. At such times the spectrum represents the pure drift motion, i.e., electron energies acquired in the process of ionization. Also, as far as the positions or relative heights of the peaks are concerned, nothing except aesthetics is usually gained by continuing the time integration after the spectrum has initially formed. For these reasons our nominal choice is the $4\frac{1}{4}$-cycle square pulse.

E. On the gauge of the electromagnetic field

It is said sometimes that the spectrum is "solved in the $\mathbf{p}\cdot\mathbf{A}$ gauge." By this we mean that one starts from the ground state of the bare Hamiltonian H_0 of (2.2), then integrates the Schrödinger equation in the form (2.6), and finally projects the result onto the eigenstates of H_0 as in (2.5). The difference from our procedure is that the wave function is not converted back to the $\mathbf{d}\cdot\mathbf{E}$ gauge using (2.8) before the spectrum is calculated. We shall briefly discuss the relation of this method to the $\mathbf{d}\cdot\mathbf{E}$ integration.

We will take the term "bare" to indicate the absence of electromagnetic fields and potentials ($A=E=0$). The bare eigenstates $|W\rangle$, and particularly the initial wave function $|\psi(t=0)\rangle$, are the same, independent of the gauge. The $t>0$ wave functions for the interacting electron are, however, different. As given in (2.8), the connection is a simple unitary transformation

$$|\psi'(t)\rangle = U(t)\,|\psi(t)\rangle\ , \tag{2.26}$$

with

$$U = e^{ixA(t)} . \tag{2.27}$$

We assume that both $A(t)$ and $E(t)$ are nonsingular at $t=0$, so the bare and interacting wave functions join smoothly there.

It will not escape attention that the predicted spectra in the two gauges, according to the conventional procedures sketched above, are generally not the same for $t>0$:

$$|\langle W|\psi'(t)\rangle|^2 \neq |\langle W|\psi(t)\rangle|^2 , \tag{2.28}$$

simply because $|\psi'(t)\rangle \neq |\psi(t)\rangle$.

The difference also has a simple interpretation. Because the unitary operator in (2.27) is the momentum translation operator, the $\mathbf{p}\cdot\mathbf{A}$ state $|\psi'(t)\rangle$ can be seen to be same as the $\mathbf{d}\cdot\mathbf{E}$ interacting state $|\psi(t)\rangle$, but with the velocity $v_A = A(t)$ added to it. As the quiver velocity $v_Q(t)$ and this fictitious transformation velocity satisfy the respective equations

$$\dot{v}_Q = E, \quad \dot{v}_A = \dot{A} = -E , \tag{2.29}$$

the sum $v_A + v_Q$ is a constant. The quiver motion of the electron is cancelled, and the $\mathbf{p}\cdot\mathbf{A}$ spectra should be frozen.

Although this argument is rigorously valid only if the electron energy is far above threshold so that $|\psi(t)\rangle$ and $|\psi'(t)\rangle$ may be approximated by simple linear combinations of left- and right-going momentum eigenstates, the freezing is quite conspicuous for all ATI peaks. In fact, the observation in our numerical experiments antedates the prediction. For an example, see Fig. 8 giving the $\mathbf{p}\cdot\mathbf{A}$ counterpart of Fig. 2 for the choice $\phi=\pi/2$, i.e., $E(t)=\mathcal{E}_0\cos\omega t$. In this case the peaks are permanently at the positions where they are found in the $\mathbf{d}\cdot\mathbf{E}$ spectrum of Fig. 2 at times corresponding to $n\pm\frac{1}{4}$ cycles.

The inequality expressed by (2.28) opens up the question of which result should be used in the subsequent analysis. Adiabatic turn-on of the fields in real experiments may well make any difference unobservable at present, but this does not diminish the importance of this question as a matter of principle. We will return to this treacherous issue elsewhere, and in this paper just adopt the widely advocated view[23] that the $\mathbf{d}\cdot\mathbf{E}$ results are the "correct" ones.

F. Restrictions on the parameters

As we have already mentioned, in our computation a characteristic ATI spectrum emerges after a few field cycles if there is ever going to be one. We have encountered two general types of situations when we do not obtain usable spectra at all.

As the field intensity is decreased, keeping the frequency and interaction time fixed, the spectrum finally becomes "erratic." An example of such a spectrum is shown in Fig. 9 for $\omega=0.148$, $\mathcal{E}_0=0.025$, and $T=180.43$. We will discuss elsewhere the interpretation of spectra at intensities low enough to see the perturbative scaling of the ATI peak heights with intensity.

Also, as the field intensity is increased, keeping the frequency and interaction time fixed, the spectrum is eventually lost in a broad background. Figure 10, which shows the spectra for the two field strengths $\mathcal{E}_0=0.07$ and 0.14 for ten-photon ionization with $\omega=0.07$, offers an example.

These problems are not entirely numeric, but reflect some underlying physics that is not fully understood at present. Effectively for every fixed frequency ω we obtain meaningful results only in a limited window of field strengths $\mathcal{E}_0$. The choice of what to regard as meaningful is naturally subjective. Our present criterion is to reject results that no longer look like ATI spectra, e.g., which do not show clearly identifiable peaks whose spacing equals the photon energy.

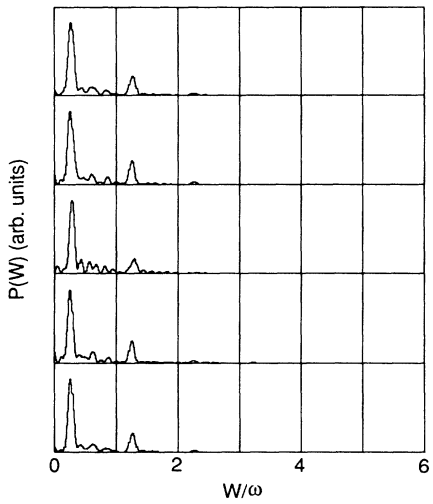

FIG. 8. Electron spectra for the field frequency $\omega=0.148$ and strength $\mathcal{E}_0=0.05$ for the square pulse of the form $\mathcal{E}(t)=\mathcal{E}_0\cos\omega t$, at times corresponding to 8, $8\frac{1}{8}$, $8\frac{1}{4}$, $8\frac{3}{8}$, and $8\frac{1}{2}$ cycles of the field (from top to bottom). These graphs are run using the $\mathbf{p}\cdot\mathbf{A}$ gauge of the dipole interaction rather than the $\mathbf{d}\cdot\mathbf{E}$ form of Fig. 2.

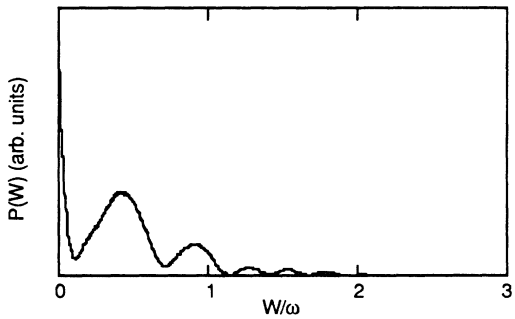

FIG. 9. Electron spectrum for a $4\frac{1}{4}$-cycle square pulse with $\omega=0.148$ and $\mathcal{E}_0=0.025$. ATI peaks cannot be identified.

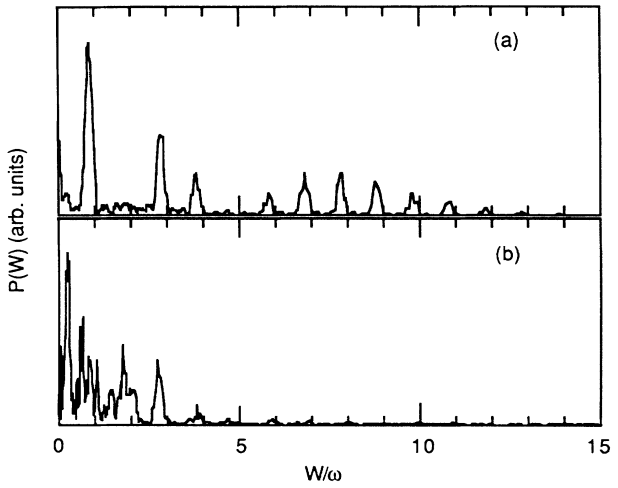

FIG. 10. Electron spectra with $\omega=0.07$ (ten-photon ionization) for square pulses with (a) $\mathcal{E}_0=0.07$, $4\frac{1}{4}$ field cycles and (b) $\mathcal{E}_0=0.14$, $8\frac{1}{4}$ cycles. These examples are fairly low-accuracy computations with $N=9000$, $\delta x=0.1$, and $\delta t=0.087\,656$.

III. ANALYSIS OF ELECTRON SPECTRA

Having explained the numerical procedures in great detail, we now turn to the findings that have emerged from study of the electron spectra. We demonstrate the ponderomotive shift of the continuum threshold, point out a free-electron scaling in our results, and contrast the simulations with two primitive Keldysh-type models. This section concludes with a partly speculative discussion of the implications of the results.

A. Shift of the continuum threshold

In real experiments the lowest-energy peaks in the spectrum are suppressed or outright vanish in comparison with the higher ones as the intensity is increased. A widely accepted explanation[13,14] combines two theoretical concepts. First, when the ejected electrons leave the laser focus, their quiver motion is converted into translational kinetic energy. They gain an energy equal to the ponderomotive potential of a charged particle in an ac field, $W_P=\mathcal{E}_0^2/4\omega^2$. Second, it is assumed that inside the field the ionization energy is dynamically shifted up from the zero-field ionization potential W_I (here $W_I=0.6698$ from Table I) by nearly the same amount W_P. The number of photons required to ionize the atom then increases from $n_0=[W_I/\omega]$ to $n_E=[(W_I+W_P)/\omega]$, where brackets mean "smallest integer larger than." The effects of the threshold shift and of the ponderomotive acceleration on the electron energies almost cancel. The photoelectron peaks emerge at the detector with energies nearly independent of the light intensity, except that the ionization channels corresponding to absorption of fewer than n_E photons are closed and the corresponding peaks are missing.

The ponderomotive after-acceleration is absent in our simulations because the field is homogeneous in the whole space and the electron never leaves the laser beam. However, the upshift of the ionization threshold should remain. Hence the peaks should move down in energy with increasing intensity. To check this argument, we plot in Fig. 11 the photoelectron spectra for $\mathcal{E}_0=0.05$, 0.070 71, and 0.085, with $\omega=0.148$ fixed. We include some negative-energy states, the highest of which still behave like part of the continuum for this interaction time $T=180.43$ corresponding to $4\frac{1}{4}$ cycles of the field. The spectra are pulled down in energy with increasing intensity. We actually see a channel close as the lowest peak sinks below the continuum limit.

By observing the peak positions and counting the channel closings we can also deduce the threshold shift quantitatively as a function of intensity. Specifically, we derive from the position W_0 (the maximum of the lowest above-threshold peak) the quantity

$$R=\frac{W_0+(n_E-n_0)\omega-(n_0\omega-W_I)}{W_P} \tag{3.1}$$

and plot it in Fig. 12 as a function of the field strength for three-, five-, and ten-photon ionization with $\omega=0.27$, 0.148, and 0.07, respectively. The error bars reflect the estimated absolute numerical accuracy of the peak positions.

If the peaks were precisely at the positions corresponding to the ponderomotive shift of the continuum threshold, $R=1$ would hold true identically. Since by its very definition $R\to 1$ as $\mathcal{E}_0\to\infty$, in the case of five-photon ionization we have explicitly checked, as in Fig. 11, that the three closings of ionization channels expected in the finite intensity range of Fig. 12 take place approximately at the intensities predicted by the ponderomotive-shift argument. The quantity R represents the ratio of the shift of the ionization threshold to the ponderomotive potential. It appears from Fig. 12 that the higher is the multiphoton order, the closer (in relative terms) is the thresh-

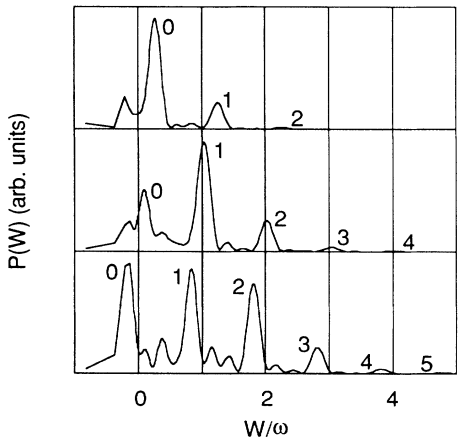

FIG. 11. Electron spectra for $\mathcal{E}_0=0.05$, 0.070 71, and 0.085 (from top to bottom) with $\omega=0.148$ fixed, for $4\frac{1}{4}$-cycle square pulses. With increasing intensity the lowest ionization channel is closed. The numbers track the corresponding peaks at different intensities.

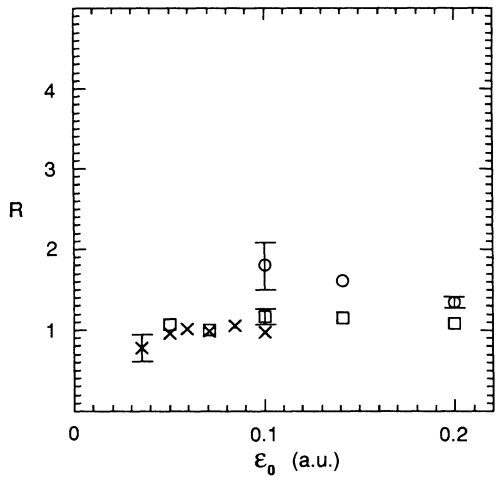

FIG. 12. The quantity R, essentially the ratio of the shift of the continuum threshold to the ponderomotive potential, as a function of the field strength $\mathcal{E}_0$ for $4\frac{1}{4}$-cycle square pulses with the laser frequencies $\omega=0.27$ (○), 0.148 (□), and 0.07 (×). The error bars reflect the estimated absolute accuracy 0.01 of the position of the lowest ATI peak.

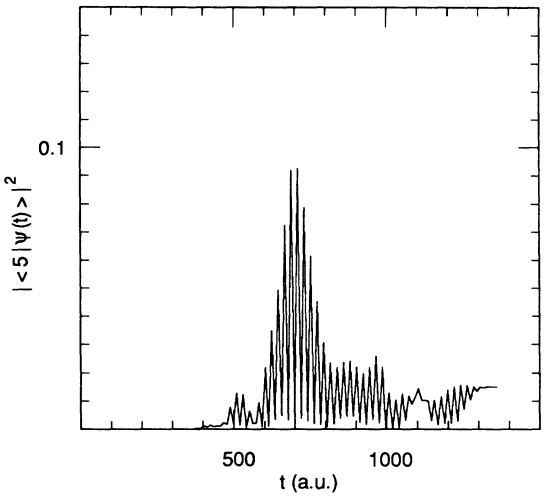

FIG. 13. Population of the fifth excited state of the atom as a function of time for a 32-cycle smooth pulse with $\omega=0.148$ and $\mathcal{E}_0=0.1$. The maximum population coincident with the maximum intensity is unusually high.

old shift to the ponderomotive potential.

Recently downshifts of the peaks have been reported[6,7] in real experiments utilizing laser pulses so short that the electrons do not have time to leave the focus before the pulse goes by. Then the ponderomotive after-acceleration is inoperative. These experiments and our numerical experiments are conceptually equivalent in that the ponderomotive acceleration is avoided at least partially, and the results are also qualitatively similar.

To conclude this section we momentarily return to the bound-level populations obtained in five-photon ionization with a 32-cycle smooth pulse for $\mathcal{E}_0=0.1$, as in Fig. 7. We have studied these populations from $n=0$ to $n=9$. It turns out that the populations of the first (the subject of Fig. 7) and *fifth* states are the largest ones among the excited states. The population of the fifth excited state $n=5$ is plotted in Fig. 13 as a function of time.

Now, in Fig. 5 for the $32\frac{1}{4}$-cycle square pulse with $\mathcal{E}_0=0.1$ the position of the lowest peak in the continuum corresponding to actual *six*-photon ionization is $W_0=0.088$, and subtracting one photon energy gives $W=-0.060$. On the other hand, by Table I the state $n=5$ is the odd-parity state whose energy is closest to -0.060. We thus interpret the anomalously large population of the fifth excited state at the maximum intensity of the pulse as an indication that the Rydberg levels slide up by an amount roughly equal to the shift of the continuum threshold; and close to the maximum of the smooth pulse the level $n=5$ is shifted to five-photon resonance.

B. Free-electron scaling of ATI spectra

To shed new light on the mechanism of ATI we next compare the ATI scaling behavior in our simulations with elementary continuum-electron concepts. The key point to notice is that the parameter $\eta=\mathcal{E}_0^2/\omega^3$, four times the ratio of the ponderomotive energy to the photon energy, is the only possible dimensionless parameter for a free, nonrelativistic, quantum mechanical electron in an external radiation field. It is thus no accident that free-electron arguments[8,24] invariably lead to scaling of ATI with this parameter. It is obvious[15] that this scaling cannot remain exactly valid in a theory where no free-electron or nearly free-electron ansatz has been made. It is an open question whether the scaling is a good approximation for an electron above the ionization threshold of a real atom.

Our wave functions and photoelectron spectra are implicitly functions of η, of course. We therefore derive from the average energy

$$\langle W\rangle=\frac{\int_0^\infty dW\, WP(W)}{\int_0^\infty dW\, P(W)} \tag{3.2}$$

of the continuum electrons and from the position W_0 of the lowest peak the dimensionless quantity

$$N=\frac{1}{\omega}(\langle W\rangle-W_0) \tag{3.3}$$

and plot it in Fig. 14 as a function of η for various field strengths for five- and ten-photon ionization (squares and crosses, respectively).

Alternatively, we could first define a peak more carefully as the region of W around the local maximum of the spectrum between the points on either side of the maximum where the monotonous decrease of $P(W)$ away from the maximum ceases, then compute the area of the peak P_S, and finally define

$$N=\frac{\sum_{S=0}^{\infty} SP_S}{\sum_{S=0}^{\infty} P_S} . \tag{3.4}$$

We use this definition in Fig. 14 for three-photon ionization (circles).

Either way, $N(\eta)$ is a measure of the number of ATI peaks. For instance, N is zero if there is only one symmetric narrow peak in the continuum. The numbers $N(\eta)$ defined in (3.3) and (3.4) normally agree to within a few tens of percent. In fact, such an agreement is one of our criteria for a valid ATI spectrum. However, because of the large area that accumulates in the background as compared to the widely spaced peaks, the definition (3.3) would occasionally give a negative N to one of the three-photon points in Fig. 14. This is why we use the definition (3.4) for three-photon data in this paper, instead of the more clear-cut expression (3.3).

For some of the ten-photon spectra used in compiling Fig. 14 the relative heights of the peaks in the spectra are already strongly corrupted by truncation errors, but $N(\eta)$ turns out to be much less sensitive to them. The data in Fig. 14 are thus believed to have a numerical accuracy of about 10%.

Another interesting question is how much the use of short $4\frac{1}{4}$-cycle pulses influences the outcome. To this end we note that in the exceptionally unfavorable case of Figs. 5 and 6 (of the positive-energy spectra we have generated, these are the only ones where the change with time is apparent even to the eye) N varies from 0.66 to 0.92, the $4\frac{1}{4}$-cycle result being the largest. This range is quite wide, but not wide enough to alter the qualitative features of Fig. 14.

Considering that the intensities of three- and ten-photon ionization for the same η differ by a factor of 50, it is clear that the number of ATI peaks primarily depends on $\mathcal{E}_0$ and ω through the combination η rather than individually on the intensity or frequency.

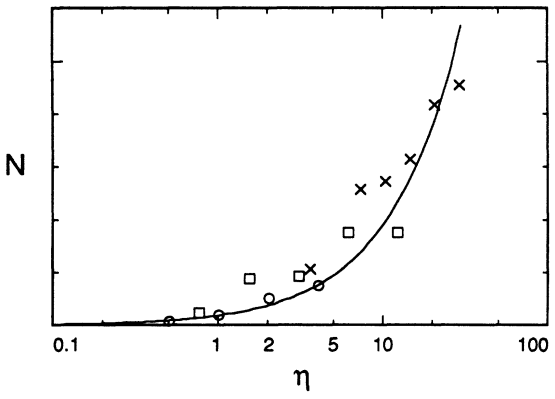

FIG. 14. Average number of above-threshold peaks N as a function of the dimensionless parameter $\eta=\mathcal{E}_0^2/\omega^3$ for $4\frac{1}{4}$-cycle square pulses, for the same three laser frequencies as in Fig. 12. The solid line is the fit to the form $N=K\eta$, giving $K=0.188$. The display is logarithmic in order to separate the data for low-η values.

C. Keldysh models of ATI

We finally compare our ATI simulations with two final-state dressing models whose key idea is originally due to Keldysh.[20] They are based on two notions: (a) the wave function of a positive-energy electron in both a laser field and the electrostatic field of its ion is approximated by a photon-dressed free-electron Volkov state and (b) lowest-order perturbation theory connects the bound initial state to the free Volkov final states.

The Volkov state[25] is the Floquet solution to the time-dependent Schrödinger equation of a free electron in the external field. In the nonrelativistic approximation, in the $\mathbf{d}\cdot\mathbf{E}$ gauge, and for the field $\mathcal{E}_0\sin\omega t$, it reads

$$\psi_p(x,t)=\exp\left\{i\left[x\left[p-\frac{\mathcal{E}_0}{\omega}\cos\omega t\right]+\frac{p\mathcal{E}_0}{\omega^2}\sin\omega t-\frac{\mathcal{E}_0^2}{8\omega^3}\sin 2\omega t-\left[\frac{p^2}{2}+\frac{\mathcal{E}_0^2}{4\omega^2}\right]t\right]\right\} . \tag{3.5}$$

Here p is the momentum such that the Volkov state turns into the plane wave $\exp(ipx)$ if the field is turned off adiabatically. The term in the first parentheses represents a plane wave whose momentum oscillates as appropriate for the quiver motion of the ion, the term in the second parentheses is the Floquet energy consisting of the bare energy of the electron and the ponderomotive shift, and the remaining terms come from the periodic part of the Floquet function. The form of the wave function (3.5) corresponds to linear polarization, the only one that can exist in one spatial dimension.

Using the generating function of the Bessel functions, the wave function may be written

$$\psi_p(x,t)=\exp\left\{i\left[\left[p-\frac{\mathcal{E}_0}{\omega}\cos\omega t\right]x\right]\right\}\times\sum_n\left\{\left[\sum_k J_{2k-n}\left[\frac{p\mathcal{E}_0}{\omega^2}\right]J_k\left[\frac{\mathcal{E}_0^2}{8\omega^3}\right]\right]\times\exp\left[-i\left[\frac{p^2}{2}+\frac{\mathcal{E}_0^2}{4\omega^2}+n\omega\right]t\right]\right\} . \tag{3.6}$$

The key feature of (3.6) is that a state whose energy at zero field equals $W=p^2/2$ is shifted up by the ponderomotive potential and acquires sidebands whose energy separation equals the photon energy. To excite an electron whose momentum outside the field were p, it is sufficient to excite any of these sidebands.

Several versions of the Keldysh model have been applied to ATI. All take their main characteristics from the Bessel functions of the Volkov states, but otherwise differ quite a lot in their strategy. In some cases it is assumed that the ground state ionizes directly.[8,9,20] In other words, high-order sidebands of continuum states are excited by one-photon transitions directly from the ground state. High-order Bessel functions describe even the lowest-order peaks in the continuum in such a theory. In other approaches[10] it is assumed that the atom jumps

over the bound states with the aid of an effective multiphoton matrix element, so that the lowest peak in the continuum has the Bessel function order zero. Intermediate forms[10] are also possible where the order of the lowest peak might equal, say, the number of channels that are closed as a result of the finite intensity. The problem with all approaches resorting to the multiphoton matrix element is that high-order effective transition matrix elements are in practice nearly impossible to calculate *ab initio*.

At the present status of Keldysh-type models one really cannot justify more elaborate treatments than the one obtained simply by using the Bessel functions (the strengths of the sidebands) as the relative heights of different peaks in the continuum:

$$H_S^v = \left| \sum_{k=-\infty}^{\infty} J_k \left[\frac{\mathcal{E}^2}{8\omega^3} \right] J_{S+v+2k} \left[\frac{p_S}{\omega^2} \right] \right|^2 . \tag{3.7}$$

We assume that the Sth (0,1, . . .) electron peak emerges with energy

$$W_S = (n_E + S)\omega - (W_I + W_P) \tag{3.8}$$

and momentum

$$p_S = (2W_S)^{1/2} , \tag{3.9}$$

both incorporating the ponderomotive shift of the threshold. The models where the ground state is coupled to the continuum directly or via an effective multiphoton matrix correspond to the respective choices $v = n_E$ and $v = 0$ in (3.7).

All matrix element factors that multiply the peak heights are taken to be independent of energy in (3.7). In particular, the prefactor does not tend to zero at the continuum threshold. This is a viable assumption for two reasons. First, we deal with energy spectra and not the flux of outgoing electrons, which would incorporate as a multiplier the asymptotic velocity that tends to zero at the continuum threshold. Second, our atom has a long-range binding potential like the Coulomb potential. Therefore, at least in one-photon transitions the oscillator strength per unit energy extrapolates continuously across the ionization threshold.[22] Models where the coupling per unit energy goes to zero at the threshold are suspect both in view of this observation and also because in our simulations the zero of energy does not seem to acquire any singularly special position.

The peak heights predicted by formula (3.7) for $v = n_E$ and $v = 0$ are shown in Figs. 15(a) and 15(b), and in Fig. 15(c) we give the corresponding *ab initio* spectrum, in all cases using $\omega = 0.07$ and $E = 0.070\,71$. The quantitative agreement between Figs. 15(a) or 15(b) with 15(c) is bad, and the modulation in the envelope of the peaks in graphs 15(b) and 15(c) is the only plausible candidate for even a qualitative similarity. The present versions of the Keldysh model do not represent accurately an atomic electron.

D. Summarizing the analysis of electron spectra

Our results on the movement of the peaks as a function of intensity strongly support the ponderomotive shift and

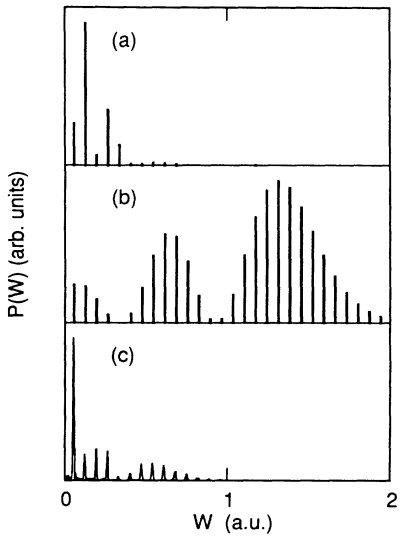

FIG. 15. Photoelectron spectra from Eq. (3.7) for $v = n_E$ (a) and $v = 0$ (b), and from the numerical simulation for an $8\frac{1}{4}$-cycle square pulse (c), with $\omega = 0.07$ and $\mathcal{E}_0 = 0.070\,71$. The simulation spectrum is computed using the iteration parameters $N = 15\,308$, $\delta x = 0.070\,71$, and $\delta t = 0.011\,219\,9$. For these parameters the individual peak heights sustain truncation errors $\sim 30\%$ and the total ionization (~ 0.1) is off by $\sim 10\%$. Nonetheless, the qualitative appearance of the spectrum is not dictated by truncation errors.

channel closing[13,14] as the mechanism of the relative suppression of the lowest peaks in the electron spectrum, which takes place in ATI experiments. We basically corroborate recent short-pulse experiments.[6,7]

Suppose next that the photon dressing of the continuum states were the dominant mechanism of ATI. Put differently, suppose that a quantitatively accurate ATI model can in principle be set up like in our primitive Keldysh-type models, but with more accurate continuum wave functions or a better account of the coupling between the bound and continuum states. High up in energy where the continuum states are only slightly perturbed by the ion core the free-electron parameter η is expected to govern the continuum dressing. The parameter η should show up prominently in the scaling of ATI with the field strength and intensity. On the other hand, light can induce transitions between the atomic continuum states only because they differ from free-electron plane waves as a result of the Coulomb interactions with the atomic core. An atom admittedly has enough dimensional quantities to make up the dimensionless η, but we consider it unlikely that a pure free-electron parameter happens to govern continuum-continuum transitions which are possible only because the electrons are not free. All told, the numerically observed free-electron scaling of ATI is nicely compatible with simple continuum dressing.[20,8–10]

Free-electron scaling might be robust enough to survive the complications of real experiments too, so it may be worthwhile to look for it specifically.

Some more speculative remarks about the Keldysh

models might also be warranted. No Keldysh model built on free-electron wave functions can be reliable close to the threshold where the electrons feel the ionic core strongly. Indeed, the region around zero energy is different in all three Figs. 15. Second, if the notion of an effective multiphoton matrix element is viable in the first place, one would expect the coupling to behave somewhat like the cross section of the photoelectric effect, i.e., tend to zero as the continuum energy increases. The true heights of the ATI peaks as a function of the electron energy should eventually fall off faster than in models based on constant coupling. In fact, the relation between Figs. 15(b) and 15(c) is as suggested by this reasoning, whereas the agreement between 15(a) and 15(c) becomes worse still if the peaks in 15(a) are multiplied by a function that falls off with energy. Third, when 15(a) and 15(c) are both multiplied by the square root of energy in the calculation of the energy flux, the agreement might become reasonable, and a coupling that tends to zero at the continuum threshold could render the agreement even better. Such a coupling, however, does not appear plausible.

The η scaling of the Keldysh-type models may also be of some interest. High up in electron energy the momentum of the peak S is accurately given by $p_S=(2S\omega)^{1/2}$, which thus is a feasible overall approximation for the momenta if there are many peaks present. In the case $v=0$ (multiphoton matrix element replacing the bound states) the peak heights from (3.7) may be written

$$H_s^0=\left|\sum_{k=-\infty}^{\infty} J_k\left[\frac{\eta}{8}\right] J_{S+2k}(\sqrt{2S\eta})\right|^2 . \tag{3.10}$$

With the assumption $p_S=(2S\omega)^{1/2}$ we have removed from the theory the last trace of atomic structure, namely the dependence of the peak positions on ionization energy. It is no surprise then that (3.10) is a function of η and S alone. Using the peak heights from (3.10) as the areas P_S in (3.4), we obtain numerically for large η the expression for the number of peaks

$$N(\eta)=\tfrac{1}{2}\eta . \tag{3.11}$$

For comparison, the slope of the linear fit in Fig. 14 is 0.19. On the other hand, in the $v=n_E$ type Keldysh model the true η scaling (independent of the ionization potential) sets in when $W_P \gg W_I$. Such parameters are currently not accessible in our numerical simulations.

IV. TURN-ON TRANSIENTS IN ELECTRON SPECTRA

The recent observation[7] of spectral structure within the ATI peaks broke new ground in multiphoton ionization physics. In their paper Freeman *et al.* explain the intra-peak features with time-dependent level shifts: The pulse intensity varies as a function of time, and so do the level shifts. At some intensities a bound level is brought to an intermediate resonance, which manifests itself in an increased ionization rate and an extra peak in the spectrum. We have so far not been able to reproduce this chain of events in our simulations. Instead, we have discovered another mechanism that creates multiple peaks within the ATI peaks.[26]

In Fig. 16 we plot a portion of the photoelectron spectrum for the $64\frac{1}{4}$-cycle square pulse with $\mathcal{E}_0=0.05$, and with $\omega=0.52$ corresponding to two-photon ionization. As the energy range shown spans just one photon energy, the multiple peaks cannot be ascribed to ATI.

To exhibit the origin of the structure in Fig. 16 we give in Fig. 17 the same spectrum, part of the energy level diagram of the atom and a few possible light-induced resonance transitions, all drawn to scale. The middle peak labeled 0″ in the spectrum of Fig. 16 corresponds to two-photon ionization of the ground state, while the rest of the peaks (including the largest one) come from one-photon ionization of excited bound states. The laser nearly matches the frequency from $|0\rangle$ to $|2\rangle$, but this transition is dipole forbidden and no resonance ensues.

We discuss these observations in a semiquantitative model. We start by assuming that the light first couples the ground state $|0\rangle$ to the other bound states $|n\rangle$ ($n=1,2,\ldots$), and in the second step the excited bound states $|n\rangle$ to the various continuum states $|W\rangle$. The respective dipole-moment matrix elements are denoted by d_{0n} and d_{nw}, and the coupling energies by Ω_{0n} ($=d_{0n}\mathcal{E}_0/2$) and Ω_{nw}. The rotating-wave approximation (RWA) is the second ingredient of our approach. We first replace the level energies with their detunings from resonance; when the ground-state energy is redefined as zero, the excited state $|n\rangle$ will have the energy $\Delta_n=W_n+W_I-\omega$, and the continuum state $|W\rangle$ the energy $\Delta_w=W+W_I-2\omega$. Second, the couplings between the levels become time independent. The couplings after the two-step RWA are sketched in Fig. 18.

Let us treat the light-induced coupling between the bound states as a small perturbation. To first order the ground state acquires a small admixture of excited-state character, and the excited states receive a small ground-state component. Time-independent perturbation theory gives as the "dressed" energy eigenstates

$$|0'\rangle=|0\rangle+i\sum_n \frac{\Omega_{0n}}{\Delta_n}|n\rangle, \quad |n'\rangle=|n\rangle-i\frac{\Omega_{0n}}{\Delta_n}|0\rangle . \tag{4.1}$$

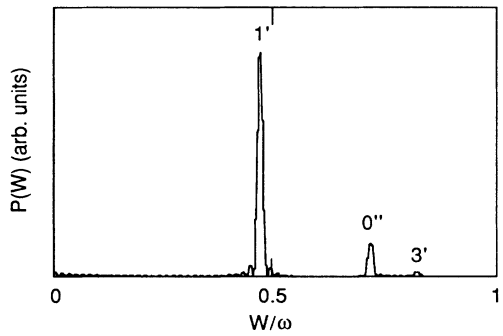

FIG. 16. Structure within the first ATI peak for a $64\frac{1}{4}$-cycle square pulse ($T=776.34$) with $\mathcal{E}_0=0.05$, and with $\omega=0.52$ corresponding to two-photon ionization. The total ionization is 1.4×10^{-2}. The notation refers to the physical origin of the peaks: See Fig. 17 and the text.

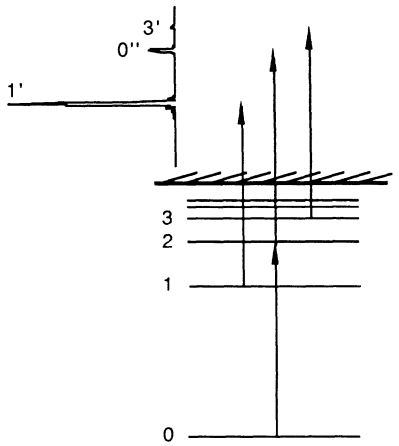

FIG. 17. ATI spectrum of Fig. 16, part of the energy level diagram of the atom, and a few possible light-induced resonance transitions, all drawn roughly to scale. It is apparent that the peak 0'' in Fig. 16 originates from two-photon ionization of the ground state $|0\rangle$, while the peaks denoted by 1' and 3' come from one-photon ionization of the excited bound states $|1\rangle$ and $|3\rangle$.

In second order the levels also shift, but this is of no concern here.

The coupling to the continuum causes an (exponential) decay of the dressed states and accompanying accumulation of electron energy peaks in the continuum. The peaks corresponding to ionization of $|0'\rangle$ and $|n'\rangle$ will have the bare energies $2\omega - W_I$ and $\omega + W_n$, respectively, and Fermi's golden rule gives the transition rates

$$\Gamma_0 = 2\pi \left| \sum_n \frac{\Omega_{0n}\Omega_{n,2\omega - W_I}}{\Delta_n} \right|^2, \quad \Gamma_n = 2\pi \Omega^2_{n,\omega + W_n} . \tag{4.2}$$

Γ_0 is recognized as the usual two-photon ionization rate from time-dependent perturbation theory (within the RWA).

In the numerical experiment of Fig. 16 the field is turned on suddenly at the initial time $t = 0$. We therefore decompose the ground state $|0\rangle$ in terms of the dressed states, whose populations to lowest order in the field intensity are

$$|\langle 0' | 0\rangle|^2 = 1, \quad |\langle n' | 0\rangle|^2 = \frac{\Omega^2_{0n}}{\Delta^2_n} . \tag{4.3}$$

Subsequently these dressed states decay exponentially to the continuum. The total populations of the corresponding electron spectrum peaks as a function of time are

$$P_0 = 1 - \exp(-\Gamma_0 t), \quad P_n = \frac{\Omega^2_{0n}}{\Delta^2_n}[1 - \exp(-\Gamma_n t)] . \tag{4.4}$$

After a long enough time when all exponentials have decayed out, the ratio of the populations in the "energy-nonconserving" (P_n) and "energy-conserving" (P_0) peaks is proportional to the field intensity, the small parameter of the perturbation theory.

A more interesting situation occurs when the relevant dressed levels have not yet decayed significantly,

$$\Gamma_0 t, \Gamma_n t \ll 1 . \tag{4.5}$$

Then (4.2), (4.4) give

$$P_0 = 2\pi \left| \sum_n \frac{\Omega_{0n}\Omega_{n,2\omega - W_I}}{\Delta_n} \right|^2 t ,$$
$$P_n = 2\pi \left| \frac{\Omega_{0n}\Omega_{n,\omega + W_n}}{\Delta_n} \right|^2 t . \tag{4.6}$$

As long as the inequality (4.5) is not violated, the ratio of the peak heights remains unchanged both as a function of time and when the intensity of the field is varied. If the coupling matrix elements were slowly varying functions of continuum energy so that the difference between $2\omega - W_I$ and $\omega + W_n$ would not be crucial, the energy-nonconserving peaks would give the incoherent decomposition of the two-photon transition rate. Also, in the weak-field limit of perturbation theory $\mathcal{E}_0 \to 0$ the extra peaks become infinitely long lived. This is the reason we dub them energy nonconserving.

In our numerical experiments we find that up to $T = 776.34$ ($64\frac{1}{4}$ cycles of the field, ~ 20 fs) and $\mathcal{E}_0 = 0.05$ ($\sim 10^{14}$ W/cm^2) the relative peak heights remain practically unchanged with changing interaction time and field strength. This is as expected in view of the fact that $\Gamma_1 T = 1.8$ and $\Gamma_3 T = 0.3$ hold true for the upper limits of T and $\mathcal{E}_0$.

The structure of the spectrum in Fig. 16 is thus a turn-on transient. If the field is turned on infinitely slowly, the state $|0\rangle$ transforms into $|0'\rangle$ adiabatically, and no other dressed state is populated. The energy-conserving peaks are the only ones to remain. This prediction is essentially confirmed in Fig. 19, where the electron spectrum is plotted for the $64\frac{1}{4}$-cycle square pulse and 96-cycle smooth pulse. The extra peaks, and their ATI du-

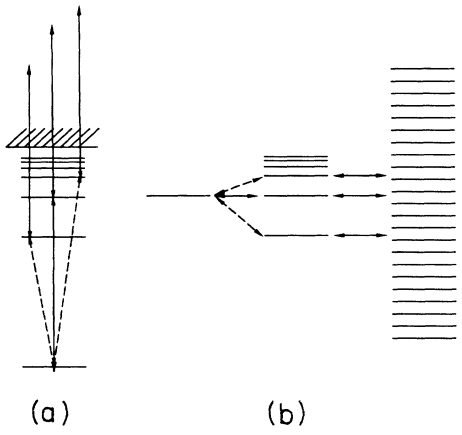

FIG. 18. The coupling scheme where the ground state is first dipole coupled to the excited bound states and these bound states are subsequently coupled to the continuum (a); the same scheme after the RWA has pulled the excited levels down by ω and the continuum by 2ω (b).

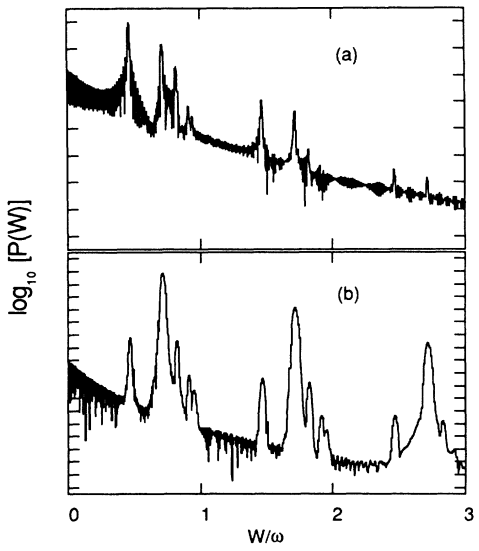

FIG. 19. Base-ten logarithm of the photoelectron spectra for a $64\frac{1}{4}$-cycle square pulse (a) and for a 96-cycle ($T=1159.97$) smooth pulse (b), for two-photon ionization with $\omega=0.52$ and $\mathcal{E}_0=0.05$. Every tick mark on the vertical scale corresponds to one decade in $P(W)$. The dynamic range is thus much larger in the smooth-pulse trace (b). The total ionizations are, respectively, 1.4×10^{-2} and 7.2×10^{-4}.

plicates, are present in both spectra, but for the smooth pulse they are strongly suppressed.

The extra peaks in the spectrum are an example of a rather esoteric way of how time-dependent perturbation theory may fail, and in principle at least they also provide a method to obtain information about the bound states of the atom. Nonetheless, in real experiments the pulses turn on smoothly, so it may be doubted whether such effects can be observed. In fact, the time scale of even our smooth pulse in Fig. 19 is much shorter than in any published experiment.

We note that we have used two-photon ionization as our example because (i) our programs then allow us to run a large number of field cycles, and (ii) we have not observed such *unambiguously identifiable* turn-on transients for five- or ten-photon ionization. In real experiments two-photon transitions may be the worst case for turn-on transients. For large multiphoton orders the time scales are automatically longer because the field period is longer. Even more importantly, the (virtual or real) intermediate levels are higher up in the Rydberg ladder and may have neighbors close by that can be excited nonresonantly. With the quest toward shorter pulses the possibility of bound-state transients in the electron spectra should be borne in mind.

The remaining question is why we apparently do not see transients for five- and ten-photon ionization. We suspect that turn-on transients or the absence thereof may be a major factor in determining the window of parameters where we see meaningful spectra. But, as a result of the required interaction times, at present it is difficult if not impossible to verify such an assumption for five- and ten-photon ionization.

V. CONCLUDING REMARKS

In this work we have laid down a procedure to carry out ATI experiments numerically, demonstrated in our simulations the threshold shift and channel closing suggested[13,14] as a possible mechanism of the peak suppression, pointed out a free-electron scaling[8,24] of the number of ATI peaks with the intensity and frequency of the field, compared two Keldysh-type[20,8–10] final-state dressing models with our numerical experiments, and demonstrated energy-nonconserving peaks in the spectrum between the ATI peaks.

Generally, our *ab initio* simulations are both laborious and cost a lot of computer time. We have thus been forced to some tradeoffs, such as using fairly short square pulses for the mass production of data, and sacrificing on the numerical accuracy. However, all our spot checks with different pulse lengths, shapes, and phases consistently suggest that in the range of parameters of our ATI spectra the electron leaks out of the atom in an essentially time-independent way, i.e., the correlation time scale of ionization is still much shorter than the time scales in our numerical experiments. The conclusions of our analysis of the electron spectra should thus remain virtually unchanged if either longer square pulses or smooth pulses were used in the simulations.

We regard the major question in our simulations to be that, without knowing why, we obtain sensible electron spectra only in a limited region of parameters. We are presently considering ways to increase substantially the interaction time available in our computations, in the hope that we would obtain new insight into the underlying physics. Another appealing project would be to improve upon the Keldysh-type theories, especially tailoring them to our one-dimensional atom, in order to see if a quantitative agreement with simulations might eventually be reached.

ACKNOWLEDGMENTS

We acknowledge grants for computer time from the John von Neumann Center that made this work possible, and another grant from the Allied-Signal Corporation for local computer equipment that made it a lot easier. One of us (J.J.) expresses his gratitude to Department of Physics and Astronomy of the University of Rochester where his part of this work was initiated.

[1]P. Agostini, F. Fabre, G. Mainfray, G. Petite, and N. K. Rahman, Phys. Rev. Lett. **42**, 1127 (1979).

[2]P. Kruit, J. Kimman, H. G. Muller, and M. J. van der Wiel, Phys. Rev. A **28**, 248 (1983).

[3]L. A. Lompré, A. L'Huillier, G. Mainfray, and C. Manus, J. Opt. Soc. Am. B **2**, 1906 (1985); U. Johann, T. S. Luk, H. Egger, and C. K. Rhodes, Phys. Rev. A **34**, 1084 (1986).

[4]H. J. Humpert, H. Schwier, R. Hippler, and H. O. Lutz, Phys.

Rev. A **32**, 3787 (1985); M. Bashkansky, P. H. Bucksbaum, and D. W. Schumacher, Phys. Rev. Lett. **59**, 274 (1987).

[5]R. R. Freeman, T. J. McIlrath, P. H. Bucksbaum, and M. Bashkansky, Phys. Rev. Lett. **57**, 3156 (1986).

[6]P. Agostini, J. Kupersztych, L. A. Lompré, G. Petite, and F. Yergeau, Phys. Rev. A **36**, 4111 (1987).

[7]R. R. Freeman, P. H. Bucksbaum, H. Milchberg, S. Darack, D. Schumacher, and M. E. Geusic, Phys. Rev. Lett. **59**, 1092 (1987). See also J. H. Eberly and J. Javanainen, Phys. Rev. Lett. **60**, 1346 (1988).

[8]H. R. Reiss, Phys. Rev. A **22**, 1786 (1980); J. Phys. B **20**, L79 (1987).

[9]M. Lewenstein, J. Mostowski, and M. Trippenbach, J. Phys. B **18**, L461 (1985).

[10]A. Dulcic, Phys. Rev. A **35**, 1673 (1987); W. Becker, R. R. Schlicher, and M. O. Scully, J. Phys. B **19**, L785 (1986); R. Shakeshaft and R. M. Potvliege, Phys. Rev. A **36**, 5478 (1987).

[11]M. Crance and M. Aymar, J. Phys. B **13**, L421 (1980).

[12]Z. Bialynicka-Birula, J. Phys. B **17**, 3091 (1984); M. Edwards, L. Pan, and L. Armstrong, Jr., *ibid.* **18**, 1927 (1985); Z. Deng and J. H. Eberly, J. Opt. Soc. Am. B **2**, 486 (1985).

[13]H. G. Muller, A. Tip, and M. J. van der Wiel, J. Phys. B **16**, L679 (1983); M. H. Mittleman, *ibid.* **17**, L351 (1984); A. Szöke, *ibid.* **18**, L427 (1985); S.-I. Chu and J. Cooper, Phys. Rev. A **32**, 2769 (1985); S.-I. Chu and R. Y. Yin, J. Opt. Soc. Am. B **4**, 720 (1987).

[14]An increase in ionization energy occurs only for states of the atom whose polarizability is negligible compared to the free-electron polarizability. See L. Pan, L. Armstrong, Jr., and J. H. Eberly, J. Opt. Soc. Am. B **3**, 1319 (1986) for a careful discussion of the so-called ponderomotive potential in a real atom.

[15]J. Javanainen and J. H. Eberly, J. Phys. B **21**, L93 (1988).

[16]R. V. Jensen and S. M. Susskind, in *Atomic and Molecular Processes with Short Intense Laser Pulses,* edited by A. D. Bandrauk (Plenum, New York, 1988), p. 253.

[17]S. Geltman, J. Phys. B **10**, 831 (1977); H. S. Antunes Neto, L. Davidovich, and D. Marchesin, in *Coherence and Quantum Optics V,* edited by L. Mandel and E. Wolf (Plenum, New York, 1984); K. C. Kulander, Phys. Rev. A **35**, 445 (1987); **36**, 2726 (1987); C. Cerjan and R. Kosloff, J. Phys. B **20**, 4441 (1987); M. S. Pindzola and C. Bottcher, J. Opt. Soc. Am. B **4**, 752 (1987).

[18]G. Casati, B. V. Chirikov, D. L. Shepelyansky, and I. Guarneri, Phys. Rev. Lett. **57**, 823 (1986); J. N. Bardsley, B. Sundaram, L. A. Pinnaduwage, and J. E. Bayfield, *ibid.* **56**, 1007 (1986); R. Blümel and U. Smilansky, *ibid.* **58**, 2531 (1987).

[19]A. Goldberg, H. M. Schey, and J. L. Schwartz, Am. J. Phys. **35**, 177 (1967).

[20]L. V. Keldysh, Zh. Eksp. Teor. Fiz. **47**, 1945 (1964) [Sov. Phys.—JETP **20**, 1307 (1965)].

[21]W. H. Press, B. P. Flannery, S. A. Teukolsky, and W. T. Vetterling, *Numerical Recipes: The Art of Scientific Computing* (Cambridge University Press, Cambridge, 1986).

[22]U. Fano and J. W. Cooper, Rev. Mod. Phys. **40**, 441 (1968).

[23]K.-H. Yang, Ann. Phys. (N.Y.) **101**, 62 (1976); D. H. Kobe and A. L. Smirl, Am. J. Phys. **46**, 624 (1978); R. R. Schlicher, W. Becker, J. Bergou, and M. O. Scully, in *Quantum Electrodynamics and Quantum Optics,* edited by A. O. Barut (Plenum, New York, 1984), p. 405.

[24]R. Shakeshaft, J. Opt. Soc. Am. B **4**, 705 (1987).

[25]D. M. Wolkow, Z. Phys. **94**, 250 (1935); L. S. Brown and T. W. B. Kibble, Phys. Rev. A **133**, 705 (1964); J. H. Eberly, in *Progress in Optics,* edited by E. Wolf (North-Holland, New York, 1969), Vol. VII, p. 361; J. H. Eberly, in *Quantum Optics,* edited by A. Kujawski and M. Lewenstein (Reidel, Dordrecht, 1986); Q. C. Su and J. H. Eberly, Phys. Rev. A **35**, 2962 (1987).

[26]J. H. Eberly and J. Javanainen, Phys. Rev. Lett. **60**, 1346 (1988).